THE JOURNAL OF PHYSICAL CHEMISTRY C

Article

pubs.acs.org/JPCC

Molecular Dynamics Simulations of Proton Transport in 3M and Nafion Perfluorosulfonic Acid Membranes

Ying-Lung Steve Tse,[†,∥,⊥] Andrew M. Herring,[†,‡] Kwiseon Kim,[§] and Gregory A. Voth*[,∥]

[†]Renewable Energy Materials Research Science and Engineering Center, and [‡]Department of Chemical and Biological Engineering, Colorado School of Mines, Golden, Colorado 80401, United States

[§]Computational Science Center, National Renewable Energy Laboratory, Golden, Colorado 80401, United States

[∥]Department of Chemistry, James Franck Institute, and Computation Institute, University of Chicago, Chicago, Illinois 60637, United States

Supporting Information

ABSTRACT: Proton transfer and local structures in 3M (EW 825) and Nafion (EW 890) membranes are investigated in this study by both standard nonreactive molecular dynamics and the self-consistent iterative multistate empirical valence bond method, which is capable of simulating multiple reactive protons and accounting for the Grotthuss mechanism of proton transport. The Nafion and 3M systems have the same backbone, so we can isolate and compare the effect of the different side chains by calculating the radial distribution functions (RDFs), self-diffusion constants, and other properties for three hydration levels at 5, 9, and 14 at 300 and 353 K. The conformations of the 3M and Nafion side chains are also compared. We found that even though many results are similar for both F3C and SPC/Fw water models, certain trends such as the sulfonate clustering can depend on the water model selected. The relationship between the different RDFs for the sulfonate, water, and hydronium is discussed. The self-diffusion constants of water for both membranes are found to be close with respect to each water model selected, even though the experimental values for 3M at 300 K are higher. The calculated self-diffusion constants of the excess protons are found to be higher for 3M than Nafion for hydration levels 9 and 14 at 300 K but statistically the same at 353 K.

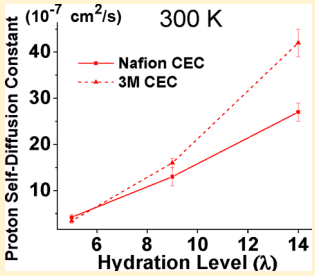

1. INTRODUCTION

A fuel cell is an electrochemical cell that converts the chemical energy of a fuel into electrical energy through a chemical reaction with an oxidizing agent.[1] Of all fuel cells, proton exchange membrane fuel cells (PEMFCs) have received particular attention for their environmental friendliness, fast start-up at low temperatures (about 80 °C), and quick response to power demands, making them an attractive option for cars and portable devices.[2] The proton exchange membrane in a PEMFC acts as an electrolyte, and its durability and conductivity play important roles for the lifetime and performance of the fuel cell. Most PEMFCs today use perfluorosulfonic acid (PFSA) membranes. In the late 1960s, DuPont discovered Nafion, which has since become the most well-known PFSA membrane. Much has been learned about many macroscopic properties of these PFSA membranes, especially Nafion, over the years from experiments.[3] Resolving the molecular details of how these membranes operate is not easy with current experimental techniques, but computer simulations can directly probe the atomic length scales while providing greater control of the conditions such as the membrane backbone structures, hydration levels, and temperature for comparison.

Understanding proton transport in proton exchange membranes can lead to new designs with better durability and conductivity. It is now known that proton transport involves at least two key mechanisms, vehicular and hopping (Grotthuss) mechanisms.[4] The latter is caused by the rearrangement of chemical bonds. Ab initio calculations would be a natural choice to study proton transport because electrons are explicitly taken into account, but the length and time scales that can be studied are too short to capture the relevant features of proton exchange membranes. Larger length and time scales are accessible to classical molecular dynamics simulations, but bonding arrangements are fixed in classical nonreactive force field methods so they cannot describe the Grotthuss mechanism. In order to get a more accurate description of proton transport in classical molecular dynamics, a force field has to account for the constantly changing bonding topology for chemical reactions in which O−H chemical bonds are formed and broken. One such method that has had considerable success is the multistate empirical valence bond (MS-EVB) theory.[5−8] Simulating multiple excess protons with the original MS-EVB models was a challenge because of its $O(N^m)$ order of complexity, where N is the number of EVB states and m is the number of excess protons. A more recent extension to MS-EVB, called self-consistent iterative MS-EVB or SCI-MS-EVB,[9] has made it possible to simulate multiple protons with computational cost that scales linearly with the

Received: January 21, 2013
Revised: April 3, 2013

   dx.doi.org/10.1021/jp400693g | J. Phys. Chem. C XXXX, XXX, XXX−XXX

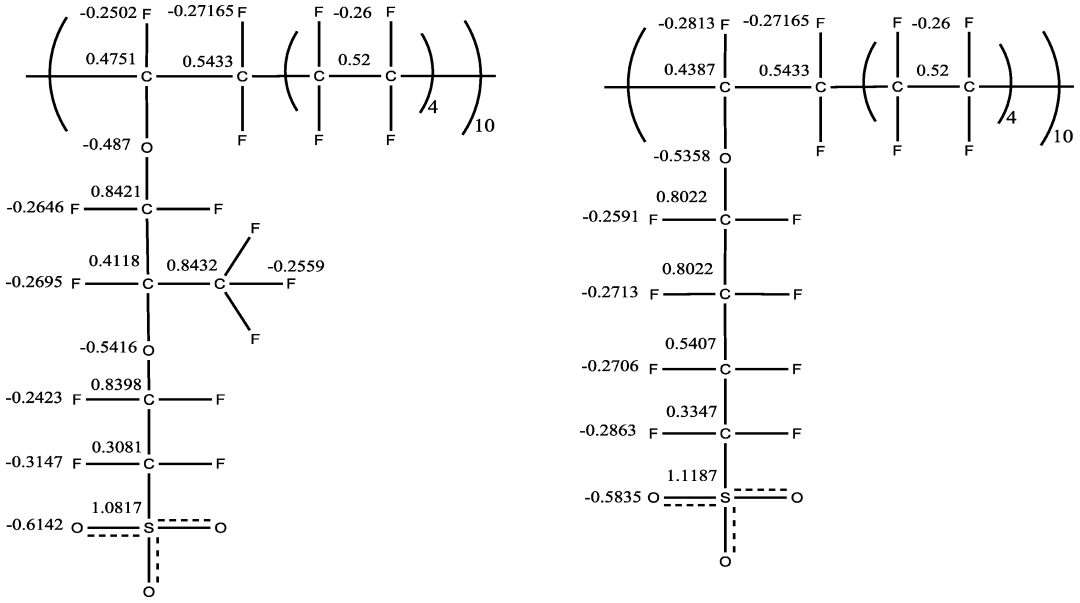

Figure 1. Structures of Nafion 890 (left) and 3M 825 (right). The number next to an atom is the partial charge used in the simulations.

number of excess protons. This method is crucial in the study of acidic systems such as PFSA membranes.

Modifications to the pendant side chains can lead to improved mechanical strength and conductivity performance. Two such examples are Hyflon (some different names for it are Dow, Aquivion, or SSC membrane) and 3M PFSA membranes, both of which have a shorter side chain than Nafion.[10,11] Experiments have shown that Hyflon and the 3M membrane with equivalent weight of about 900 or lower have better conductivity than Nafion. Additionally, the 3M membrane was shown to have a greater than 15-fold increase in durability under accelerated fuel cell test conditions when compared with similar commercial PEMs.[12] There have been simulation efforts[13−15] to compare the structural and dynamical properties between Nafion and Hyflon. Even though interesting results for the 3M membrane have been obtained from DFT and DPD calculations,[16−18] no comparison has yet been made between Nafion and 3M using atomistic molecular dynamics simulations. Comparing the structural properties and proton transport of 3M with those of Nafion is the main focus of this paper. The simulation details are given in section 2, results and discussion in section 3, and finally the conclusions in section 4.

2. SIMULATION DETAILS

Two PFSA membranes, Nafion and 3M, were simulated. Their structures in the simulations are shown in Figure 1.

The membranes were inserted into their simulation box with a random morphology by a Monte Carlo algorithm that was developed by Knox and Voth[19] (in that paper, their "rp" setup was most similar to our setups here). The simulations were performed using the MD package LAMMPS[20] with our own module for SCI-MS-EVB calculations. We studied three hydration levels (λ) at 5, 9, and 14 and two different temperatures at 300 and 353 K. Each simulation box had four polymer chains of either 3M or Nafion. In order to focus on the differences in the side chains only, both 3M and Nafion systems had the exact backbone as shown in Figure 1. Additional C−F atoms were added to the ends of the backbone so that the equivalent weight (EW) for 3M was as close to 825 g/mol as possible (the number came out to be about 822 g/mol). With the same backbone as 3M, the EW for Nafion was about 890 g/mol. From this point on, we call the EW 825 3M membrane "3M 825" and the EW 890 Nafion "Nafion 890".

When the hydration level is greater than 3, it has been shown[21−24] that all the sulfonic acid groups are deprotonated to form sulfonates, so all the sulfonic acid groups were ionized in our simulations, and there were 40 excess protons in each simulation box.

The DREIDING force field[25] was used to model the membranes. Coulombic interactions were treated by standard Ewald summations,[26] with a cutoff distance 14 Å and an Ewald sum precision 10^{-5}. The partial charges for the CF backbone and the 3M side chain were obtained from a Mulliken population analysis[27] on the optimized structures at the DFT B3LYP 6-31** level in Gaussian 09[28] and are shown in Figure 1. The partial charges of the Nafion side chain and all the bond force constants for both 3M and Nafion were taken from ref 29. The force constants for angle bending followed those of ref 30. The equilibrium bond lengths and angles used were from our DFT B3LYP 6-31** calculations. For the Lennard-Jones interactions, the parameters were taken from ref 29. The Lorentz−Berthelot mixing rules and a cutoff distance 14 Å were used. The parameters for the dihedrals in the CF backbone followed those of ref 29 which were adopted from ref 31. The default DREIDING force field parameters were used to describe the remaining dihedrals.

For MS-EVB calculations, the MS-EVB3 model[8] with the self-consistent iterative algorithm[9] for multiple excess protons was used. The MS-EVB3 model was developed to use with the SPC/Fw water model.[32] To compare with other classical MD simulation data in the literature, nonreactive simulations using the F3C water model[33] were also performed.

For initial equilibration steps, the MS-EVB (reactive) potential was not turned on. A 1 fs time step was used for all simulations. The systems were first relaxed using constant NPT dynamics at 400 K and 1 atm for 6 ns. The systems were then cooled down to the desired temperature (300 or 353 K) at the same pressure for another 6 ns with constant NPT dynamics.

dx.doi.org/10.1021/jp400693g | J. Phys. Chem. C XXXX, XXX, XXX−XXX

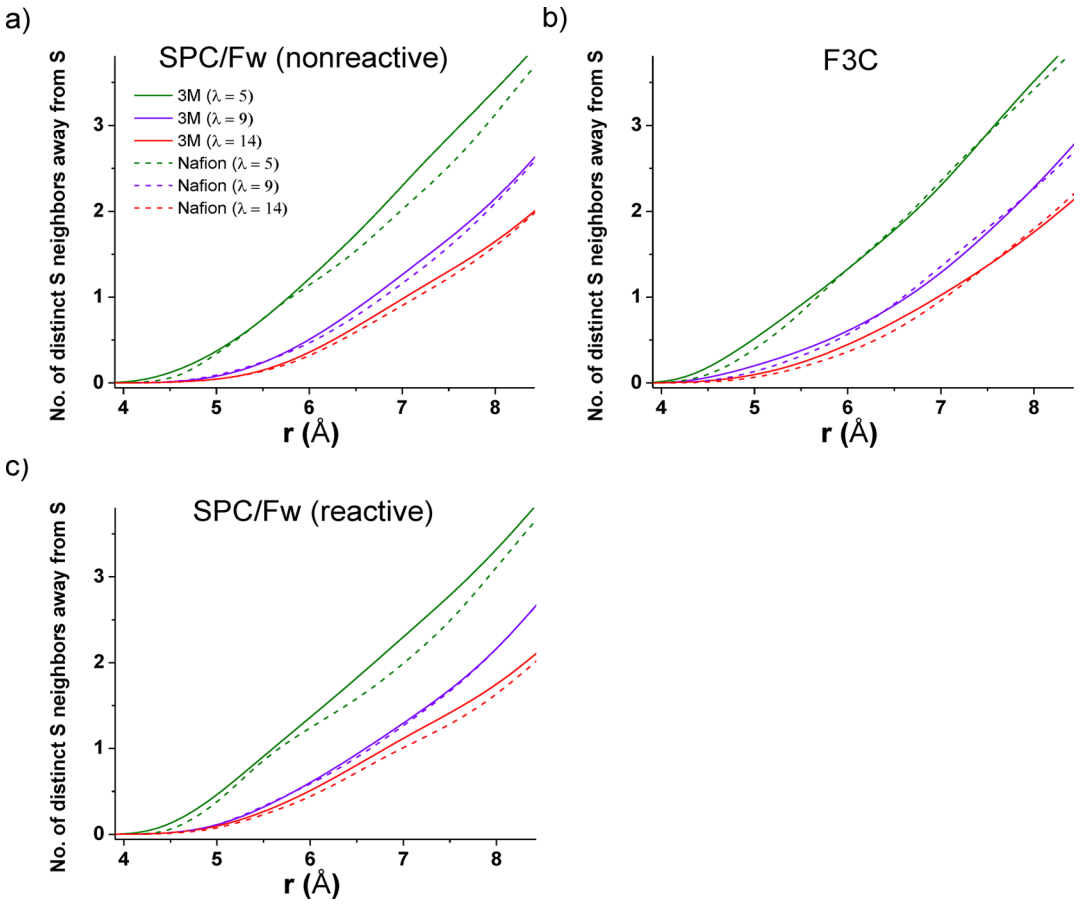

Figure 2. (a) Coordination numbers, obtained from integration of the RDFs, as a function of hydration levels for the SPC/Fw water with nonreactive dynamics. The solid and dash lines are for 3M and Nafion, respectively. The temperature is 300 K. (b) For the F3C water (nonreactive) model. (c) For SPC/Fw with reactive dynamics (SCI-MS-EVB).

The systems were further equilibrated with constant NVT dynamics at the desired temperature for an additional 11 ns.

After equilibration, six configurations from the last 2.5 ns of the NVT trajectory were chosen to become the initial states in constant NVE simulations that followed. For classical calculations, data was then collected from six 5-ns trajectories in constant NVE dynamics. For MS-EVB calculations, the structures were further equilibrated at constant NVT with the reactive potential turned on for 200 ps, before data for each system was collected from six 1-ns constant NVE trajectories.

3. RESULTS AND DISCUSSION

In this section, we look at different equilibrium and dynamical properties for 3M and Nafion and compare their differences. The local interactions, described by the RDFs, between two sulfonate sulfurs (S−S), between sulfonate sulfur and water oxygen (S−OW), and between sulfonate sulfur and hydronium oxygen (S−OH) as well as the size of water clusters provide information about the local environment felt by the protons. The RDF between sulfonate and proton center of effect charge (S−CEC) is last introduced because it can be seen as an extension of the RDF S−OH. Since the main focus in this paper is to study the differences coming from the side chains, their distributions of conformations are also studied and compared. Finally, dynamical quantities such as the mean-squared displacements (MSDs) of water and proton CEC are analyzed. From the MSDs, the water and excess proton self-diffusion constants are then calculated and can be directly compared with experimental data.

Density. The density values after equilibration range from 1.54 to 1.79 g/cm^3. As hydration level (λ) increases, the membrane "swells" more and its density decreases. As expected, the density decreases as temperatures increases. Using either water model gives very similar densities. All the density values are shown in the Supporting Information (Table S1).

Coordination Numbers of Sulfonate Sulfurs Away from a Sulfonate Sulfur (S−S). By comparing the coordination numbers obtained from the integrations of the S−S radial distribution functions (RDFs), one can learn about the sulfonate clustering. Figure 2 shows the coordination numbers for both 3M and Nafion as a function of hydration level at temperature 300 K. Three setups, SPC/Fw (nonreactive), F3C (nonreactive), and SPC/Fw (reactive) water, are studied. For completeness, their RDFs are given in the Supporting Information (Figure S1). In all three cases, increasing the hydration level increases the separation between two sulfonate groups. Increasing the hydration level increases the size of water domains for which the average end-to-end distance between two side chains also becomes larger.

Whether the separation between two sulfonate groups is larger or shorter for Nafion than 3M depends on the hydration level, the distance range, and, interestingly, the water model selected. For nonreactive SPC/Fw water, the coordination numbers are almost identical for hydration levels 9 and 14 until r reaches 5.5 Å. For r > 5.5 Å, there is more clustering for 3M

dx.doi.org/10.1021/jp400693g | J. Phys. Chem. C XXXX, XXX, XXX−XXX

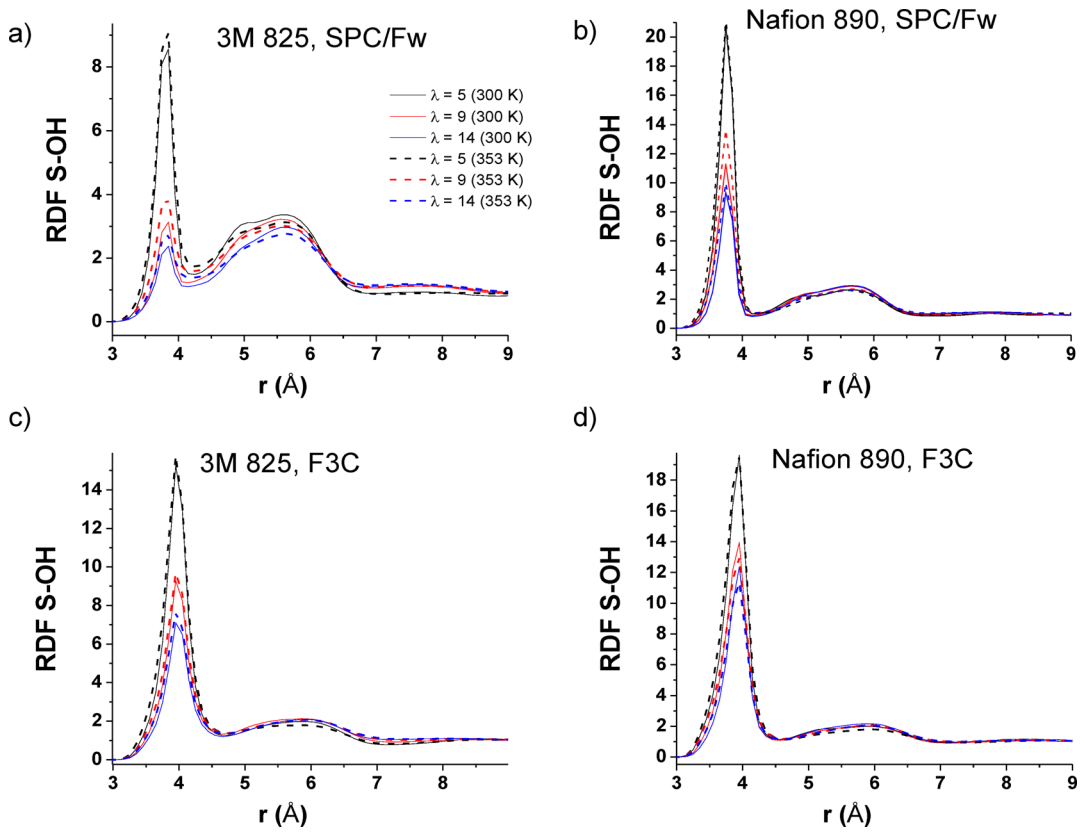

Figure 3. (a) RDF for 3M between sulfonate sulfur and hydronium oxygen with SPC/Fw water. (b) RDF for Nafion with SPC/Fw water. (c) RDF for 3M with F3C water. (d) RDF for Nafion with F3C water.

Table 1. Coordination Numbers for SPC/Fw Water and Hydronium in the First Solvation Shell around a Sulfonate Sulfur Which Is Defined To Be between 0 and 4.25 Å

	no. of hydronium oxygens in the range of 0−4.25 Å from sulfonate sulfur, SPC/Fw.				no. of SPC/Fw water in the range of 0−4.25 Å.			
λ	3M 300 K	3M 353 K	Nafion 300 K	Nafion 353 K	3M 300 K	3M 353 K	Nafion 300 K	Nafion 353 K
5	0.70	0.78	1.24	1.32	4.10	3.90	3.49	3.41
9	0.28	0.36	0.66	0.81	5.13	4.95	4.91	4.59
14	0.20	0.24	0.47	0.54	5.39	5.30	5.31	5.07

than Nafion. For hydration level 5, there tends to be more clustering for 3M except at around 5.5 Å where clustering is about equal for both membranes. However, when the selected water model is F3C, there is clearly more clustering in 3M than Nafion for $r < 6$ Å for all three hydration levels, but no clear trends for levels 5 and 9 for $r > 6$ Å. Even though it is hard to confirm how the S−S distances differ in the two membranes without experimental data, what is shown here is that the interactions between the sulfonates and water play an important role in sulfonate clustering. Such comparison for sulfonate clustering was made for Hyflon and Nafion previously by Karo et al.,[34] Devanathan and Dupuis,[15] and Lui et al.[14] The first two references in which the F3C water model was used found there is more clustering in Hyflon, whereas Lui et al. who used a flexible TIP3P water model found more clustering in Nafion. The different water models selected might have attributed to the discrepancy, similar to the differences that were observed here between SPC/Fw and F3C for Nafion and 3M.

Figure 2c shows the MS-EVB data for reactive SPC/Fw water. We found that reactive hydrated proton dynamics generally have only a small impact on the RDFs and the corresponding coordination numbers. For this reason, except for quantities that are related to the hydrated proton center of excess charge (defined later), RDFs from only nonreactive data are shown.

RDF between Sulfonate Sulfur and Hydronium Oxygen (S−OH). The nonreactive results are presented in Figure 3. The hydronium cations were treated as classical nonreactive particles (for related reactive results, please see the S−CEC RDF later in this section).

SPC/Fw results are first discussed. For 3M, the RDFs at all hydration levels show two distinct peaks, a sharp peak at about 3.8 Å and a broad peak at about 5.6 Å. The locations of the two peaks are related to the first two hydration shells in which the hydronium ions reside. As hydration is increased to higher levels, the height of the sharp peak decreases significantly. If we look at the coordination number in the first solvation shell which is defined to be between 0 and 4.25 Å (see the left side of Table 1), it decreases from 0.70 to 0.28 and 0.20 from $\lambda = 5$ to 9 and 14. This means the hydronium tends to be further away from a sulfonate and interacts more strongly with water. As temperature increases from 300 to 353 K, the coordination numbers in the first solvation shell increase. This trend has to

dx.doi.org/10.1021/jp400693g | J. Phys. Chem. C XXXX, XXX, XXX−XXX

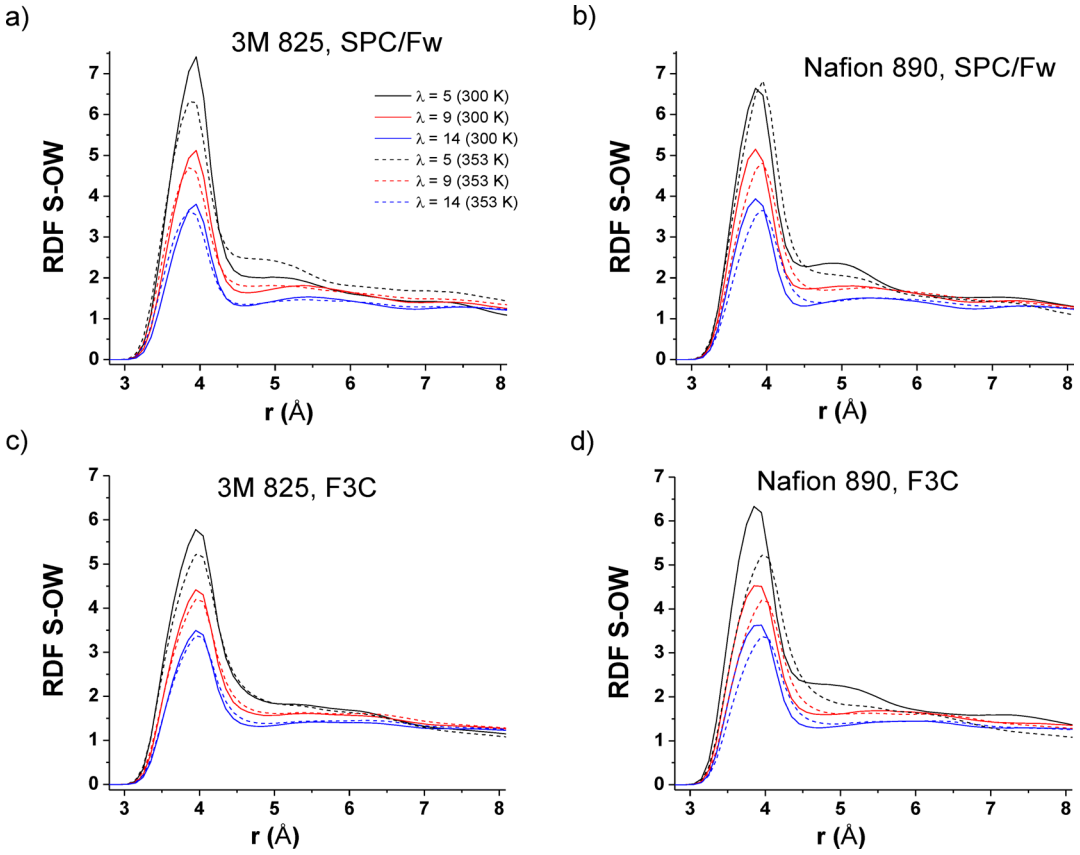

Figure 4. (a) RDF for 3M between sulfonate sulfur and SPC/Fw water oxygen. (b) RDF for Nafion with SPC/Fw water. (c) RDF for 3M with F3C water. (d) RDF for Nafion with F3C water.

do with the number of water neighbors clustering around a sulfonate as we will see next. When there is more water competing for the attention of the sulfonate groups and hydronium ions, there seems to be less attraction between the sulfonate and the hydronium.

For Nafion, the same tall and broad peaks like those of 3M are present, but the tall peak has a much higher height than that of the 3M peak under the same conditions. This partially has to do with the more negative partial charges used for the sulfonate oxygens in Nafion, and this causes a higher hydronium density in the first solvation shell for Nafion than 3M at all hydration levels and temperatures.

For the F3C water model, many of the trends remain the same, but the most notable difference is the width of the first peak that is considerably larger than that of SPC/Fw. The coordination number for the first peak is twice as large for F3C (see the Supporting Information, Table S2) when compared to SPC/Fw, implying there is a stronger attraction between the sulfonate and the hydronium in the F3C than in the SPC/Fw water model. The same RDFs for Nafion have been reported in ref 34 and are consistent with our results.

RDF between Sulfonate Sulfur and Water Oxygen (S−OW). The results of SPC/Fw are first discussed (Figures 4a and b). For 3M, there is a distinct peak at 4 Å and a broad peak from about 4.5 to 6.5 Å. These two peaks represent the first two hydration shells. Because most hydronium ions reside in these two solvation shells, the locations of these two peaks roughly determine the locations of the two peaks in the S−OH RDF. We see from Table 1 that the coordination number of water increases as the hydration level is increased. The effect of increasing the temperature slightly decreases the coordination number in the first solvation shell, which is likely due to the increased mobility of water.

For Nafion, the general features of the RDF are similar to those of 3M, even though the broad peak at hydration level 5 at 300 K is more distinct. The coordination numbers up to 4.25 Å are 3.5, 4.9, and 5.3 for λ = 5, 9, and 14 at 300 K which are all lower than those of 3M at the same temperature. This implies that water is more spread out for Nafion, and this will be discussed in more detail later in the section when we analyze the closest distance from a water molecule to a sulfonate.

When we compare the coordination numbers of water and hydronium ions (see Table 1) around a sulfonate sulfur, it is interesting to see that they have opposite trends; *the higher the water coordination number around a sulfonate, the lower the hydronium coordination number.* This seems to hold true when we compare the same membrane at the different temperatures or different membranes at the same temperature. There seems to be a competition between water and hydronium for the sulfonates.

F3C water gives very similar results (Figures 4c and d). The coordination numbers for F3C water and hydronium are in the Supporting Information (Table S2). The observation that there is an opposite trend for the two coordination numbers also seems to hold within statistical errors.

Estimate of Relative Sizes of Water Clusters. The S−OW RDF and Table 1 show that the coordination number of water around a sulfonate in the first solvation shell is higher for 3M than Nafion. Since the number of water molecules is constant at a given hydration level, the water clusters in Nafion

dx.doi.org/10.1021/jp400693g | J. Phys. Chem. C XXXX, XXX, XXX−XXX

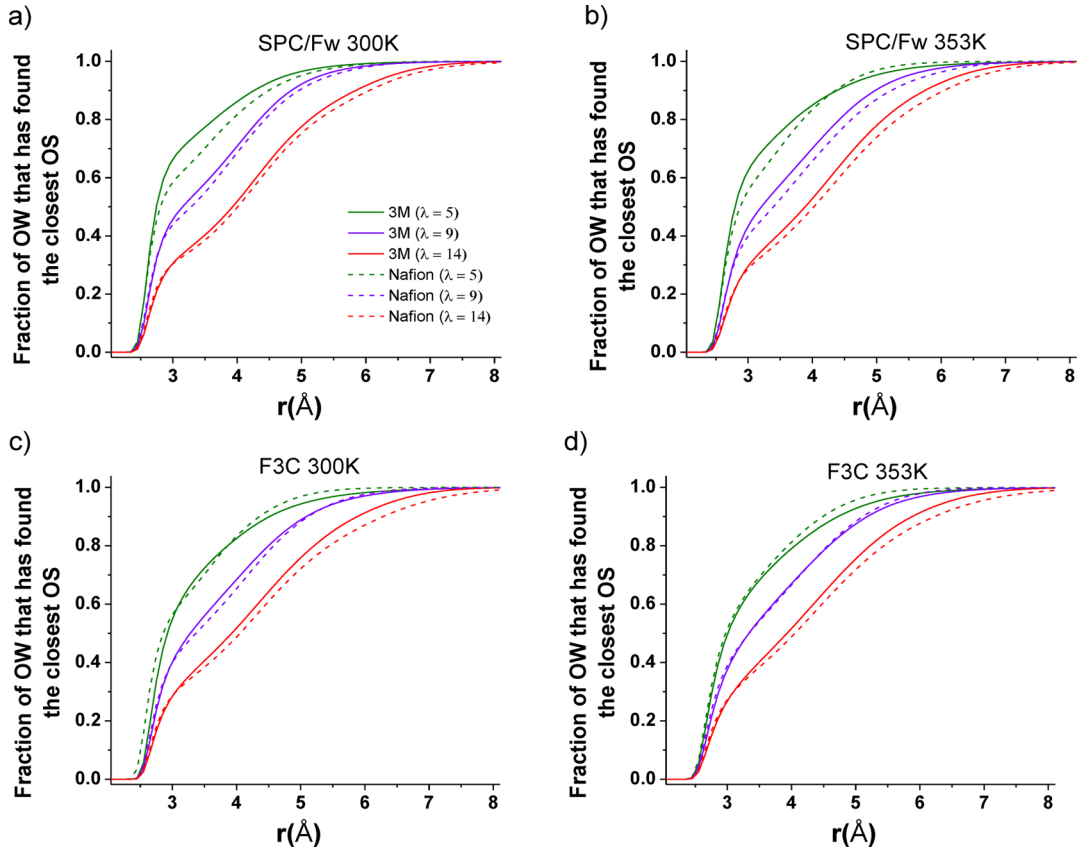

Figure 5. (a) Fraction of water oxygen (OW) as a function of the distance to its closest sulfonate oxygen (OS). SPC/Fw water at 300 K. (b) SPC/Fw water at 353K. (c) F3C water at 300 K. (d) F3C water at 353 K.

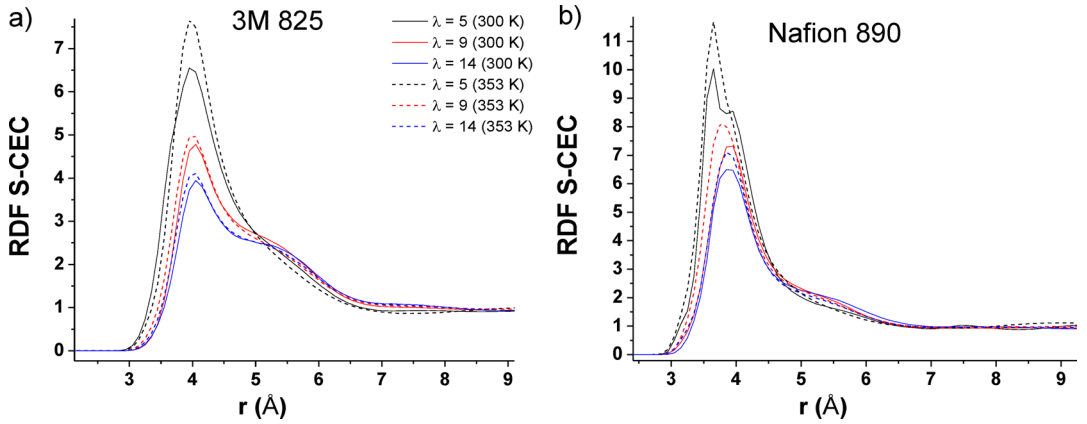

Figure 6. (a) RDF for 3M between sulfonate sulfur and hydrated proton CEC. (b) Same RDF for Nafion.

tend to be bigger and more spread. One way to estimate the size of a water cluster is to study the shortest distance from each water to its closest sulfonate oxygen. Devanathan and Dupuis[15] estimated the radius of a water cluster using the upper limit of these shortest distances. Here, we estimated the relative sizes of water clusters by studying the cumulative probability distribution of the shortest distance as shown in Figure 5. For SPC/Fw water at 300 K, all the 3M curves increase faster than the Nafion ones, and this means the water molecules can find their closest sulfonate oxygen more easily in 3M on the average. The curves reach almost a fraction of 1 at about 6, 7, and 7.5 Å for hydration levels 5, 9, and 14; there is only a very small population of water molecules left that are more than 8 Å away from their nearest sulfonate oxygen neighbor. At 353 K for SPC/Fw water, all the curves are shifted slightly to the right for the fact that the water clusters are more spread at a higher temperature. At this higher temperature, there is no longer a clear trend for hydration level 5; the water in 3M is able to find their closest sulfonate neighbors at shorter distances than in Nafion, but the trend is reversed for $r > 4.5$ Å.

For F3C water, the features are similar, except that there is no clear trend for hydration level 5 at both temperatures, even though Nafion seems to have larger water clusters than 3M for levels 9 and 14.

RDF between Sulfonate Sulfur and the Hydrated Proton Center of Excess Charge (S−CEC). The calculations

dx.doi.org/10.1021/jp400693g | J. Phys. Chem. C XXXX, XXX, XXX−XXX

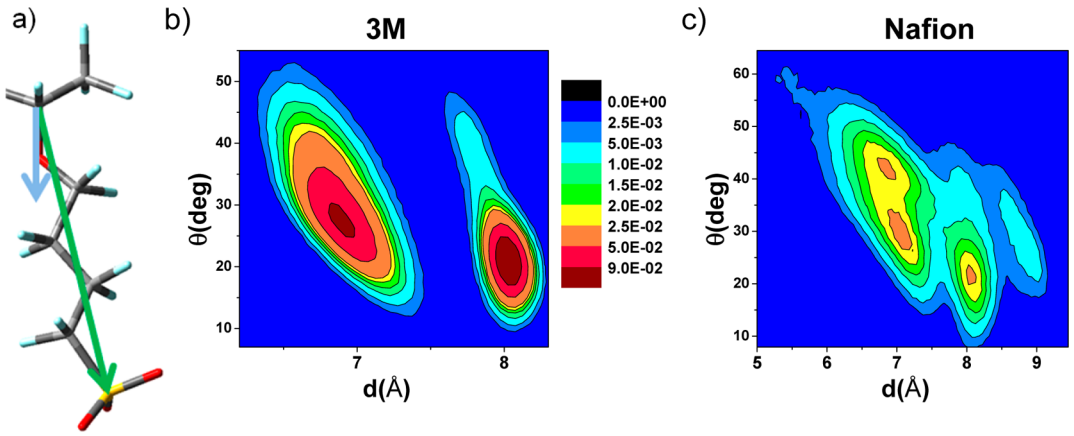

Figure 7. (a) Green arrow starts from the carbon at the joint of the backbone and side chain to the sulfonate sulfur. Blue arrow starts from the carbon at the joint and points in the direction to the ether oxygen. d is defined to be the length of the green arrow, and θ is the angle between the green and blue arrows. (b) Joint probability density distribution of d and θ for the 3M side chain as a contour map. The range of probability density values for each color is shown in the legend. The bin sizes for d and θ are 0.05 Å and 1.25°, respectively. The water model is SPC/Fw, the temperature is 300 K, and the hydration level is 9. (c) Same contour map for Nafion.

of the RDF between S and the hydrated proton center of excess charge (CEC) discussed here require the use of the SCI-MS-EVB calculations. Because MS-EVB3 is parametrized using the SPC/Fw water, all the data found in this subsection were generated only with the SPC/Fw water model. The introduction of the CEC is required because in an EVB formulation, unlike a classical nonreactive force field, an excess proton is not located at a single location but at multiple locations with different probability values assigned. The location of the excess charge can be more accurately described as a weighted average of all possible MS-EVB states. The definition of the position vector of a CEC is therefore given by[8]

$$\mathbf{r}_{\mathrm{CEC}} = \sum_{i=1}^{N} c_i^2 \mathbf{r}_{\mathrm{COC}}^i \tag{1}$$

where $\mathbf{r}^i_{\mathrm{COC}}$ is the position vector of the center of charge of the hydronium cation of the ith EVB state, c_i^2 is the probability weight for the ith EVB state, and N is the number of EVB states.

The results of the RDF between S and CEC are shown in Figure 6. This RDF looks similar to the RDF between S and hydronium oxygen (S−OH) (Figure 3), because they are very much related to each other. The relationship is that a classical hydronium can be approximated as the *pivot* hydronium that has the largest EVB probability amplitude. Instead of putting all the weight in a single hydronium at a definite location when we count in the calculation of the RDF between S and OH, the RDF between S and CEC is similar to counting multiple possible locations of the hydronium ion weighted by their corresponding probability. Therefore, the peaks in the RDF between S and CEC are always broader than those in the RDF between S and OH. The S−CEC RDFs for 3M have one peak at about 4 Å and a shoulder from 4.8 to 6.5 Å, and they originate from the same peaks in S−OH RDF. But now, because of the delocalized nature of excess charge by MS-EVB, the RDF is less structured and the two peaks are broader. As temperature increases, the height of the first peak increases for the same reasons why the first peak of RDF S−OH increases. As we shall see from the diffusion data that is presented later, a higher temperature yields a faster diffusion constant for the CEC. One might think a faster-moving CEC would have a more delocalized RDF, but this is not the case as we can see in the figure. It seems that there is not a clear relationship between the height of the peak and the magnitude of the diffusion constant.

For Nafion, there are also a peak near 4 Å and a shoulder from 4.8 to 6.5 Å, but because of the scale of the vertical axis, the shoulder is not very noticeable. If we compare the peak heights in the Nafion RDFs with those of 3M, we can predict that the peak in the Nafion S−OH RDF would be higher than that of 3M, and this is indeed the case. Moreover, both S−CEC and S−OH RDFs show smaller second peak/shoulder for Nafion.

Conformations of the Side Chains. To study the conformations of a side chain, we first define two metrics to describe how much the side chain is extended and how bent it is toward the backbone.

We call the carbon at the joint of the backbone and the side chain "C1". The quantity d is defined to be the distance from C1 to the sulfur and is presented as the length of the green arrow in Figure 7a. If d is larger, it means the chain is more extended. The blue arrow in the figure is a vector whose direction points from C1 to the ether oxygen. We define θ to be the (unsigned) angle between the green and the blue arrows. When θ is 0°, the chain can be thought of as totally straight. The larger the angle, the more bent toward the backbone is the side chain.

Figures 7b and c show the joint probability density distributions of d and θ as contour maps. Since the distributions do not vary significantly between the different water models, hydration levels, and temperatures studied, the data shown is from SPC/Fw water, 300 K, and hydration level 9. The first obvious difference is that the distribution for 3M is significantly more localized than that of Nafion. This has to do with the shorter 3M side chain being less flexible. Our DFT optimizations (without water) show that the d values are about 8 Å for both 3M and Nafion at zero temperature, but we see there are two favorable d distances at around 7 and 8 Å for 3M that seem to be roughly equally probable at these nonzero temperatures. At d = 8 Å, the extended 3M side chain also has smaller θ values. It has a wider range of angles when d is about 7 Å. The smaller d and larger θ values imply a bent configuration is formed. For Nafion, the preferred d and θ

dx.doi.org/10.1021/jp400693g | J. Phys. Chem. C XXXX, XXX, XXX−XXX

are not as definite, but note the fact that the most probable d and θ for Nafion match those of 3M. However, for Nafion, the probability weights in the other regions are not small and cannot be neglected. The mean of d for 3M is 7.3 Å with standard deviation (σ) 0.57 Å and that of Nafion is 7.1 Å with σ = 0.73 Å. The mean of θ for 3M is 27.1° with σ = 7.9°, and that of Nafion is 35.8° with σ = 12.2°. Within one standard deviation, there is no statistical difference between the average length of the 3M side length and that of Nafion; even though the mean θ for Nafion is larger than that of 3M, one should also keep in mind that the standard deviation is also considerably larger. If we use the relationship between the free energy and the probability, i.e., $\Delta F = -k_B T \ln(P_1/P_2)$, we see that the energy barrier for the 3M side chain to move from the local minimum at d = 7 Å to the minimum at d = 8 Å is considerably higher than that of the Nafion side chain (approximately 4 $k_B T$ vs 2 $k_B T$).

Mean-Squared Displacements and Diffusion Constants. The self-diffusion constant of water is an important quantity because it is one of the few observables that can be directly compared between simulation and experiment. Through pulsed-field gradient spin−echo NMR (PFGSE-NMR) experiments, the self-diffusion constant of water in PFSA membranes can be estimated. On the other hand, in MD simulations, the self-diffusion constant of a particle, like a water molecule, can be estimated by studying its MSD which is defined to be

$$\mathrm{MSD}(t) = \frac{1}{N}\left\langle \sum_{i=1}^{N} |\mathbf{r}_i(t) - \mathbf{r}_i(0)|^2 \right\rangle \tag{2}$$

where the angular brackets denote an ensemble average of systems whose initial conditions are sampled from a canonical (NVT) distribution and propagate in time with constant NVE dynamics.

A sample MSD plot of SPC/Fw water as a function of time and hydration level is shown in Figure 8. For large time separations, the MSD of a diffusing particle scales linearly as t. In log−log scale, the slope of a MSD curve approaches to 1 from below.

With MSD scaling linearly as t at long times, one can then estimate the self-diffusion constant by the well-known Einstein formula:

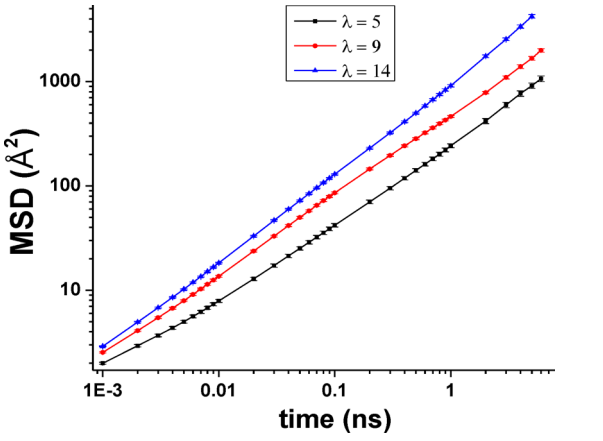

Figure 8. MSD plot of SPC/Fw water as a function of time for Nafion 890 at λ = 5, 9, and 14 at 353 K.

$$D = \lim_{t\to\infty} \mathrm{MSD}(t)/6t \tag{3}$$

In practice, the infinite time limit for the ratio cannot be obtained but instead is replaced by a convergent ratio as shown in Figure 9. The error bars for the data are statistical error

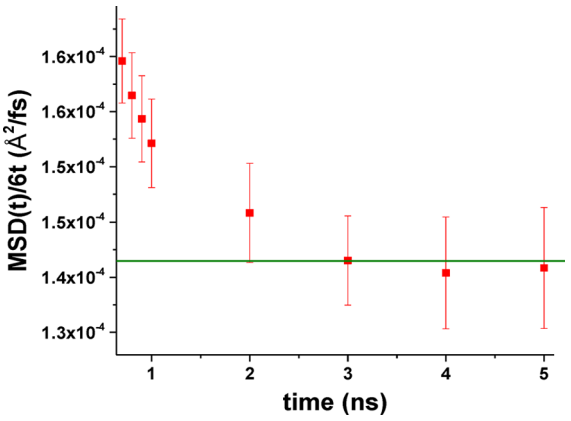

Figure 9. MSD(t)/6t as a function of t. The plot helps determine the earliest time at which the diffusion constant can be extracted. This particular example comes from the MSD of SPC/Fw water in Nafion 890 at hydration level 14 at 353 K.

estimates calculated as the standard deviation of the results for various runs divided by the square root of the number of runs. The earliest data point for the MSD(t)/6t ratio that is consistent with all the data points at longer time is chosen to be our estimate for the self-diffusion constant. In the example in Figure 9, the diffusion constant was calculated at t = 3 ns.

The diffusion constants of water for both 3M and Nafion are shown in Figure 10. Four sets of data, (1) experimental data, (2) SPC/Fw nonreactive water, (3) SPC/Fw reactive water,[35] and (4) F3C (nonreactive) water, are presented. At hydration level 5 for 300 K, the diffusion constants predicted by all water models agree well with experiment[36,37] for Nafion 1100 EW. As hydration level increases to 5 or 9 at 300 K, the diffusion constant predicted by SPC/Fw reactive water is the closest to the experimental diffusion constant, whereas SPC/Fw nonreactive water slightly underestimates it and F3C water slightly overestimates it. Typically, the order of increasing diffusion constants is F3C > SPC/Fw reactive > SPC/Fw nonreactive, except for the lowest hydration level at 5. For 3M, all water models underestimate the water diffusion constants, but the values predicted by the F3C and the SPC/Fw reactive water are closer to the experimental values at 300 K.[38] Both water models predict slower water diffusion for 3M at hydration level 5 but faster diffusion than Nafion for levels 9 and 14. This trend persists in the higher temperature at 353 K, and the water diffusion constants are roughly twice as fast.

At 300 K, the experimental 3M water diffusion constants are considerably faster than those of Nafion. Unlike the experiments, the differences between the 3M and Nafion water diffusion constants from the simulations are usually small under the same conditions, and the calculated 3M values are considerably smaller than the experimental values. *This may be evidence that the actual morphology of the experimental system is quite different from the random morphology chosen for our 3M simulations.*

One may be able to gain insight for the conductivity of a membrane by studying the motion of charged particles. In our

dx.doi.org/10.1021/jp400693g | J. Phys. Chem. C XXXX, XXX, XXX−XXX

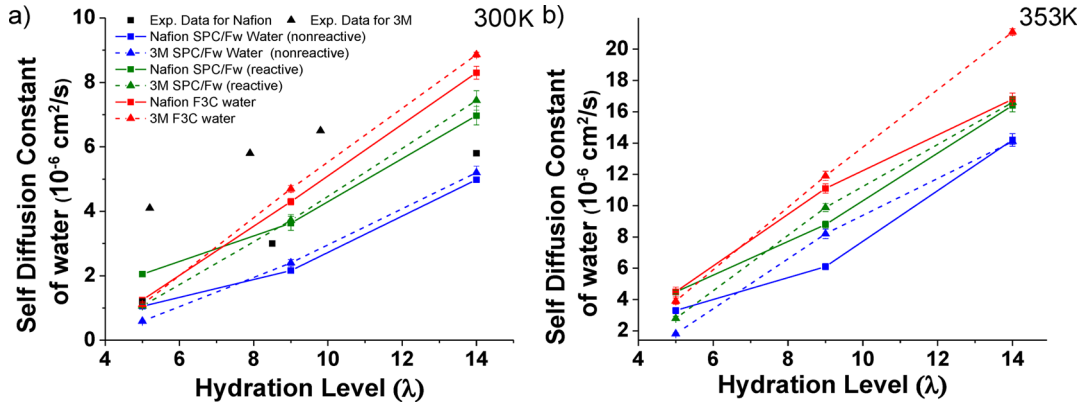

Figure 10. (a) Self-diffusion constant of water, in units of 10^{-6} cm^2/s, is plotted as a function of hydration level at 300 K. The lines are there to only guide the eye. (b) For temperature 353 K. The experimental data at 300 K for 3M is from ref 38 and that of Nafion is from ref 36 (for λ = 5, 8.5) and ref 37 (for λ = 14).

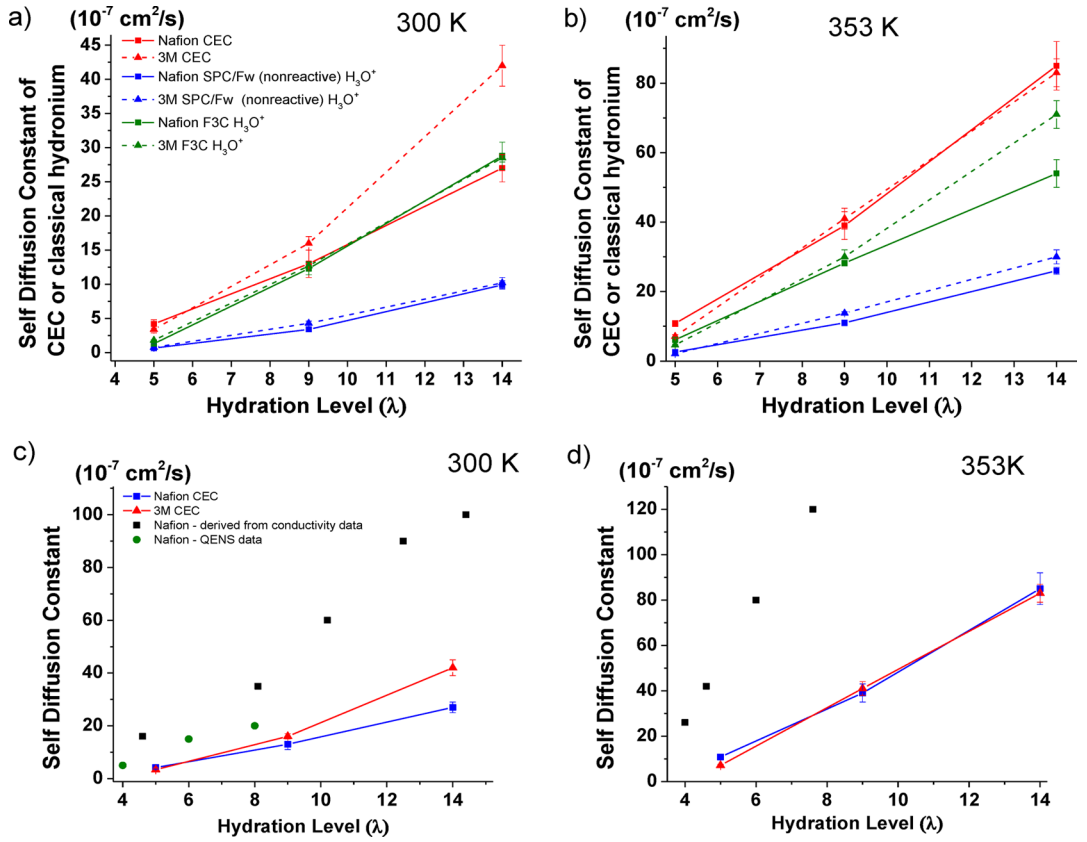

Figure 11. (a) Self-diffusion constant of the hydrated proton CEC or classical hydronium, in units of 10^{-7} cm^2/s, plotted as a function of hydration level at 300 K. (b) Same as (a), but for temperature 353 K. (c) Experimental data for Nafion[40,47] are shown along with the proton CEC diffusion constants, at temperature 300 K. (d) Same as (c), for temperature 353 K. The experimental data comes from ref 36.

case, because the anionic side chains are attached to the polymer, conductivity only comes from the motion of excess protons. With SCI-MS-EVB calculations, we can study the contributions to proton transport arising from the Grotthuss mechanism as well as the vehicular mechanism in these PFSA membranes. Direct determination of the diffusion constant of an excess proton is difficult by experiment, and so the diffusion constants are usually inferred from other measurements. Two types of experiments have been used to estimate the excess proton self-diffusion constant in a PFSA membrane: (1) conductivity and (2) quasielastic neutron scattering (QENS).[39,40] The Nernst−Einstein equation can be used to calculate the proton diffusion constant from conductivity, but one problem with using the Nernst−Einstein equation is that deviations happen when the electrolytic solution does not behave ideally,[41] and this ideality condition is not satisfied in hydrated PFSA membranes. On the other hand, from QENS measurements, Perrin et al.[40] estimated the proton diffusion constant by using a theoretical model based on Gaussian statistics and by assigning the slow protons to those of hydronium, but their interpretation rules out Grotthuss mechanism at all hydration levels, and that does not agree with other studies.[36,42,43] The values estimated by the Nernst−Einstein equation for Nafion tend to be 2−4 times larger than

dx.doi.org/10.1021/jp400693g | J. Phys. Chem. C XXXX, XXX, XXX−XXX

those of QENS. The discrepancy probably originates from the different assumptions made in the calculations as well as the processing, thermal history, and thickness of the membranes.[44,45]

Figures 11 a and b show the diffusion data for the hydrated proton CEC and classical hydronium for both water models, and Figures 11 c and d compare the diffusion constant estimates from QENS and conductivity experiments with the CEC data. For SPC/Fw water, we studied proton diffusion as classical hydronium (nonreactive, no MS-EVB) and as CEC (reactive, with MS-EVB). For 300 K, the increasing order of diffusion constant is CEC ≥ F3C classical hydronium > SPC/Fw classical hydronium for both membranes. The classical hydronium models derived from both water models have similar diffusion constants for both 3M and Nafion membranes at 300 K at all hydration levels. The 3M hydrated proton CEC has a faster diffusion constant at level 9 and 14 than Nafion but is slightly slower at level 5. Nonetheless, all models predict lower diffusion constants than both types of experiments. In particular, the hydrated proton CEC is smaller than the QENS by about a factor of 2 and is smaller than the Nernst−Einstein numbers by about a factor of 4−5; the underestimation of the diffusion constant is consistent with what was observed for an excess proton in a box of 216 SPC/Fw water molecules in the original MS-EVB3 paper[8] where the calculated classical diffusion constant of the CEC (with no quantum nuclear effects) was smaller than the experimental value for proton by about a factor of about 3. (We also note that in ref 46, the reported diffusion constants for the hydrated proton CEC in Nafion were too high because the MSD values were not correctly divided by a factor of 6, although the activation energy calculations reported in that paper were not affected by this error. After the correction for the factor of 6, the diffusion constants for the hydrated proton CEC reported in ref 46 are consistent with those reported here.) For 353 K, the increasing order of the diffusion constants predicted by different models remains the same, but both classical hydronium models predict a larger diffusion constant for 3M than Nafion at hydration levels 9 and 14. On the other hand, no statistical differences in the diffusion constants were found for the hydrated proton CEC at hydration levels 9 and 14 at 353 K, even though the CEC also diffuses faster than the classical hydronium ions.

The main difference between the hydrated proton CEC results and those of classical SPC/Fw hydronium is the involvement of the hopping (Grotthuss) mechanism. The diffusion constant of CEC is 3−7 times faster than that of SPC/Fw classical hydronium. It is therefore interesting to look more into the hopping mechanism. One way to study this is to decompose the total displacement of the CEC into a "discrete" and a "continuous" component[48]

$$\mathbf{r}_{CEC}(t) - \mathbf{r}_{CEC}(0) = \Delta\mathbf{r}_{CEC}(t) = \Delta\mathbf{r}_c(t) + \Delta\mathbf{r}_d(t) \quad (4)$$

$$\langle|\Delta\mathbf{r}_{CEC}(t)|^2\rangle = \langle|\Delta\mathbf{r}_c(t)|^2\rangle + \langle|\Delta\mathbf{r}_d(t)|^2\rangle + 2\langle\Delta\mathbf{r}_c(t)\cdot\Delta\mathbf{r}_d(t)\rangle \quad (5)$$

where $\Delta\mathbf{r}_c(t)$ and $\Delta\mathbf{r}_d(t)$ are the "continuous" and "discrete" components of the total displacement of the CEC, $\Delta\mathbf{r}_{CEC}(t)$.

How one might decompose the total CEC MSD is not unique. Our way of doing the decomposition is, for each CEC, we check in every disjoint 100-fs interval and see in that time interval if the CEC has hopped, resulting in a change in the identity of the most probable ("pivot") hydronium. If the CEC has hopped in the interval, the displacement that occurred in this 100-fs interval is assigned only to the discrete component, and the continuous component is not changed. Similarly, if the CEC has not hopped in the interval, the displacement in this 100-fs interval is assigned only to the continuous component, but not the discrete component. In particular, if the identity of the pivot state changes with one hop but changes back to the original identity in the time interval, the displacement is assigned to the discrete component. A typical plot for such decomposition is shown in Figure 12. Any decomposition that

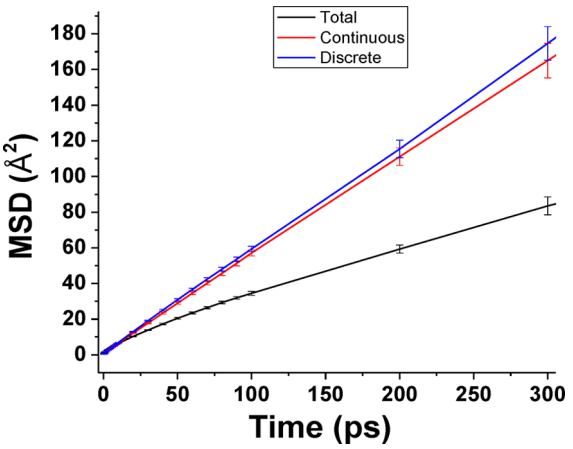

Figure 12. Sample plot for the total MSD decomposition into a continuous MSD component and a discrete MSD component. The data in this plot comes from 3M 825 at hydration level 14 and 300 K.

is similar to what is described here will show that the sum of the continuous MSD and the discrete MSD is much larger than the total MSD. In other words, the term $\langle\Delta\mathbf{r}_c(t)\cdot\Delta\mathbf{r}_d(t)\rangle$ in the equation above is negative, and this means the discrete displacement and the continuous displacement tend to move in opposite directions and partially cancel each other. This anticorrelation is not an artifact from our choice of decomposition and does not happen in a system of bulk water with an excess proton. It was first seen for Nafion in ref 48 and is now also confirmed for 3M here. The interference by the discrete component with the continuous component implies that the continuous MSD presented here cannot be the same as the vehicular MSD calculated in nonreactive MD simulations in which hopping is absent. However, by comparing the diffusion constants of proton CEC and SPC/Fw classical hydronium, we see that the overall effect of having both hopping and vehicular mechanisms contributes positively to the diffusion constant, even though the two mechanisms are anticorrelated.

To further understand the continuous and the discrete components, we have studied the MSD per one discrete or continuous move in Figures 13 a and b. We see that the MSDs are strictly increasing functions of the hydration level and temperature. We also see that the MSD per discrete hop is considerably more sensitive than the MSD per continuous move due to a change in temperature or hydration level. In particular, by increasing the temperature or the hydration level, each hop in the interval tends to be a bigger jump. This can be explained by the fact that the average separation between two water molecules increases at a higher temperature and the size of a water cluster increases at a higher hydration level as shown in Figure 4 and Figure 5.

dx.doi.org/10.1021/jp400693g | J. Phys. Chem. C XXXX, XXX, XXX−XXX

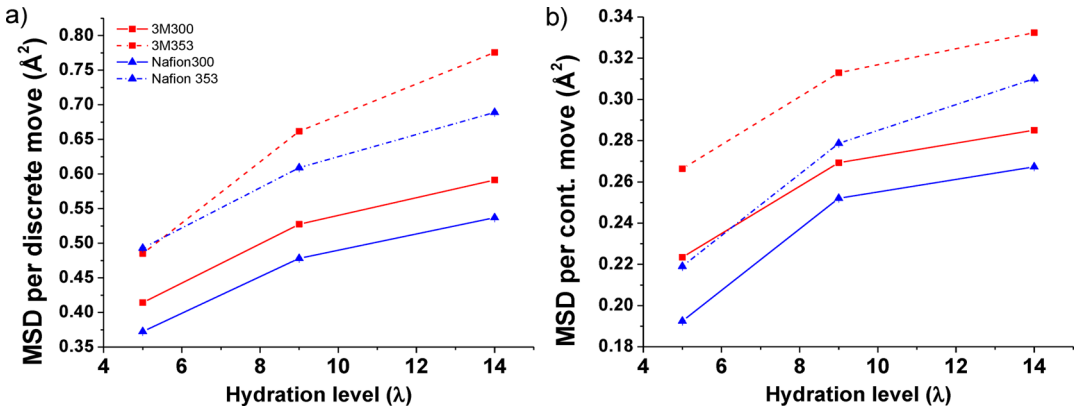

Figure 13. (a) MSD per discrete move in 100-fs interval. (b) MSD per continuous move in 100-fs interval.

4. CONCLUSIONS

The 3M membrane is the second PFSA membrane that has been investigated using the SCI-MS-EVB model. The results for different RDFs, water domain sizes, and diffusion constants were compared for 3M (EW 825) and Nafion (EW 890). In this work, both 3M and Nafion had the exact same backbone in order to better isolate the differences due to the side chains. Both SPC/Fw and F3C water models were selected; the former was needed for MS-EVB calculations, and the latter was studied to compare with the other simulations in the literature. One of the main goals in this paper is to see whether 3M and Nafion have significant differences in the structural or dynamical quantities that might explain the difference in their conductivity.

The interactions between sulfur−sulfur (S−S), sulfur−water oxygen (S−OW), sulfur−hydronium oxygen (S−OH), and sulfur−proton center of excess charge (S−CEC) are highly correlated, and this shows in the corresponding RDFs or the coordination numbers. For instance, the locations of the peaks in the S−OH RDF are roughly same as those of the S−OW RDF because the location and size of the solvation shells of water determine roughly the locations of the hydronium ions. The locations and the shapes of the peaks for S−CEC can be explained from those of S−OH because the hydrated proton CEC is a generalization of considering multiple possible locations of a hydronium ion, so the peaks for the S−CEC RDF are roughly at the same locations as those of the S−OH RDF, but they are broader because of the delocalized nature of the excess proton charged defects in the MS-EVB picture. The average S−S distance can be studied from the coordination number of distinct sulfur neighbors from a sulfonate sulfur. Many of the results are similar for the two water models. We found that whether the average S−S distance is larger or not for 3M or Nafion is sensitive to which water model is selected, even though the differences are small. Generally, whether the dynamics is reactive or not does not significantly change the RDFs that do not involve the hydrated proton CEC. When the coordination number of water around a sulfonate in the first solvation shell is higher, the coordination number of hydronium ions around a sulfonate in the first solvation shell is lower when compared to different membranes at the same temperature or to the same membrane at different temperatures, vice versa. There seems to be a competition between water and hydronium to occupy the space close to a sulfonate. From studying the distance from each water to its closest sulfonate neighbor, we found that the sizes of water clusters tend to be larger in Nafion at the higher hydration levels. Because water is more spread and there is less water in the first solvation shell around a sulfonate in Nafion, the number of hydronium ions around a sulfonate is higher.

In general, the F3C water was found to diffuse faster than both the SPC/Fw nonreactive and reactive water in the membranes under the same conditions. SPC/Fw reactive water diffuses faster than the nonreactive water. Simulations showed there is almost no difference in the self-diffusion constants of water for 3M and Nafion at hydration levels 9 and 14, even though experiments showed that water in 3M diffuses faster. *This may be evidence that the "random" morphology chosen in our simulations for 3M may not be a correct representation for the actual morphology.*

We found that the self-diffusion constant of the hydrated proton CEC is in general faster than the classical hydronium ions from both water models and the F3C classical hydronium comes in a close second. One might suspect a faster moving proton would make S−CEC RDF less structured, but it does not seem to be case because the RDF becomes more structured and yet the excess charge diffuses faster at the higher temperature. The hydrated proton CECs diffuse 3−7 times faster than the classical SPC/Fw hydronium ions because of the additional hopping mechanism. It was previously confirmed that there is anticorrelation between the hopping and vehicular mechanisms in Nafion, and we also confirmed this is the case for 3M in this paper.

The conformations of the 3M and the Nafion side chains were compared by studying the joint probability density distribution of d and θ which describe how extended and how bent the side chain is. The conformations for 3M are considerably simpler because of its shorter side chain. There are only two probable regions; one of them shows the 3M side chain is almost fully extended and straight, whereas the other region shows the side chain forms a hook. The distribution for Nafion is more delocalized because of its longer side chain. Even though the most probable distances and angles are similar to those of 3M, the other Nafion conformations have enough probability weights that they should not be neglected.

One of the most important questions to ask is why the conductivity of 3M can be as much as twice higher than that of Nafion (at 80 °C).[12,36] Previously, classical nonreactive simulations that tried to compare Hyflon with Nafion did not find any significant differences in dynamical properties.[15] There was speculation[13] that the answer would become clearer when both hopping and vehicular mechanisms are included. We did

dx.doi.org/10.1021/jp400693g | J. Phys. Chem. C XXXX, XXX, XXX−XXX

not study Hyflon, but the side chain of 3M is very similar to that of Hyflon. Fixing all other conditions except for the side chains, we found in our SCI-MS-EVB simulations that the biggest difference in the self-diffusion constants of the hydrated proton CEC for 3M is only 56% percent larger than that of Nafion at hydration level 14 at 300 K; for other hydration levels and temperature, the differences are much smaller. Therefore, we did not find evidence that the difference in the excess proton self-diffusion constants (or lack of), after taking both vehicular and hopping mechanisms into account, can explain the difference in conductivity, at least for 3M 825 and Nafion 890. We did not impose any specific morphology for the initial configurations of the membranes, and our simulation boxes were too small to account for any crystallinity. It has been suggested in a recent study by Di Noto et al.[49] that the morphology of the crystalline hydrophobic domains is crucial for the long-range proton migration in the 3M membrane. Moreover, another recent study by Feng, Savage, and Voth[50] has shown evidence that different Nafion morphology such as lamella, cylinder, or cluster can result in very different self-diffusion constants of the hydrated proton CEC. These all reinforce the idea that a more complete picture of the actual morphology of these PFSA membranes, especially as a function of equivalent weight and hydration level, is likely required to understand the differences in their proton conductivity as well as to obtain better overall agreement between the calculated values of the excess proton diffusion and the experimental measurements.

■ ASSOCIATED CONTENT

Ⓢ Supporting Information

Density values of Nafion 890 and 3M 825, RDF between two sulfonate sulfurs, and the water and hydronium coordination numbers around a sulfonate sulfur in the first solvation shell. This material is available free of charge via the Internet at http://pubs.acs.org.

■ AUTHOR INFORMATION

Corresponding Author

*Phone: 773-702-7250. Fax: 773-702-0805. E-mail: gavoth@uchicago.edu.

Present Address

[⊥]Department of Chemistry, University of Chicago, 5735 S. Ellis Ave., Chicago, IL 60637.

Notes

The authors declare no competing financial interest.

■ ACKNOWLEDGMENTS

This research was supported by the Department of Energy, Office of Basic Energy Sciences, Division of Chemical Sciences, Geosciences, and Biosciences (DOE grant DE-FG02-10ER16171 to G.A.V.), Renewable Energy Materials Research Science and Engineering Center (National Science Foundation grant DMR-0820518 to A.M.H.) at Colorado School of Mines, and the National Renewable Energy Laboratory (NREL). S.T. thanks Dr. Bryan Pivovar of NREL for very many helpful discussions.

■ REFERENCES

(1) Khurmi, R. S.; Sedha, R. S. *Material Science*; S. Chand & Co., Ltd.: New Delhi, India, 2010.

(2) Hamrock, S. J.; Yandrasits, M. A. *Proton Exchange Membranes for Fuel Cell Applications*; Technical Report 1532-1797; Taylor & Francis: New York, 2006/09/01; pp 219−244.

(3) Mauritz, K. A.; Moore, R. B. State of Understanding of Nafion. *Chem. Rev.* **2004**, *104*, 4535−4586.

(4) Kreuer, K. D. On the Development of Proton Conducting Materials for Technological Applications. *Solid State Ionics* **1997**, *97*, 1−15.

(5) Schmitt, U. W.; Voth, G. A. Multistate Empirical Valence Bond Model for Proton Transport in Water. *J. Phys. Chem. B* **1998**, *102*, 5547−5551.

(6) Schmitt, U. W.; Voth, G. A. The Computer Simulation of Proton Transport in Water. *J. Chem. Phys.* **1999**, *111*, 9361−9381.

(7) Day, T. J. F.; Soudackov, A. V.; Cuma, M.; Schmitt, U. W.; Voth, G. A. A Second Generation Multistate Empirical Valence Bond Model for Proton Transport in Aqueous Systems. *J. Chem. Phys.* **2002**, *117*, 5839−5849.

(8) Wu, Y.; Chen, H.; Wang, F.; Paesani, F.; Voth, G. A. An Improved Multistate Empirical Valence Bond Model for Aqueous Proton Solvation and Transport. *J. Phys. Chem. B* **2008**, *112*, 7146−7146.

(9) Wang, F.; Voth, G. A.; Linear-Scaling Self-Consistent, A. Generalization of the Multistate Empirical Valence Bond Method for Multiple Excess Protons in Aqueous Systems. *J. Chem. Phys.* **2005**, *122*, 144105.

(10) Maalouf, M.; Pyle, B.; Sun, C.-N.; Wu, D.; Paddison, S. J.; Schaberg, M.; Emery, M.; Lochhaas, K. H.; Hamrock, S. J.; Ghassemi, H.; et al. Proton Exchange Membranes for High Temperature Fuel Cells: Equivalent Weight and End Group Effects on Conductivity. *ECS Trans.* **2009**, *25*, 1473−1481.

(11) Kreuer, K. D.; Schuster, M.; Obliers, B.; Diat, O.; Traub, U.; Fuchs, A.; Klock, U.; Paddison, S. J.; Maier, J. Short-Side-Chain Proton Conducting Perfluorosulfonic Acid Ionomers: Why They Perform Better in PEM Fuel Cells. *J. Power Sources* **2008**, *178*, 499−509.

(12) Emery, M.; Frey, M.; Guerra, M.; Haugen, G.; Hintzer, K.; Lochhaas, K. H.; Pham, P.; Pierpont, D.; Schaberg, M.; Thaler, A.; et al. The Development of New Membranes for Proton Exchange Membrane Fuel Cells. *ECS Trans.* **2007**, *11*, 3−14.

(13) Cui, S.; Liu, J.; Selvan, M. E.; Paddison, S. J.; Keffer, D. J.; Edwards, B. J. Comparison of the Hydration and Diffusion of Protons in Perfluorosulfonic Acid Membranes with Molecular Dynamics Simulations. *J. Phys. Chem. B* **2008**, *112*, 13273−13284.

(14) Liu, J.; Suraweera, N.; Keffer, D. J.; Cui, S.; Paddison, S. J. On the Relationship between Polymer Electrolyte Structure and Hydrated Morphology of Perfluorosulfonic Acid Membranes. *J. Phys. Chem. C* **2010**, *114*, 11279−11292.

(15) Devanathan, R.; Dupuis, M. Insight from Molecular Modelling: Does the Polymer Side Chain Length Matter for Transport Properties of Perfluorosulfonic Acid Membranes? *Phys. Chem. Chem. Phys.* **2012**, *14*, 11281−11295.

(16) Clark, Ii, J. K.; Paddison, S. J.; Hamrock, S. J. The Effect of Hydrogen Bond Reorganization and Equivalent Weight on Proton Transfer in 3M Perfluorosulfonic Acid Ionomers. *Phys. Chem. Chem. Phys.* **2012**, *14*, 16349−16359.

(17) Clark, J. K.; Paddison, S. J. The Effect of Side Chain Connectivity and Local Hydration on Proton Transfer in 3M Perfluorosulfonic Acid Membranes. *Solid State Ionics* **2012**, *213*, 83−91.

(18) Wu, D. S.; Paddison, S. J.; Elliott, J. A.; Hamrock, S. J. Mesoscale Modeling of Hydrated Morphologies of 3M Perfluorosulfonic Acid-Based Fuel Cell Electrolytes. *Langmuir* **2010**, *26*, 14308−14315.

(19) Knox, C. K.; Voth, G. A. Probing Selected Morphological Models of Hydrated Nafion Using Large-Scale Molecular Dynamics Simulations. *J. Phys. Chem. B* **2010**, *114*, 3205−3218.

(20) Plimpton, S. Fast Parallel Algorithms for Short-Range Molecular Dynamics. *J. Comput. Phys.* **1995**, *117*, 1−19.

(21) Paddison, S. J.; Elliott, J. A. Molecular Modeling of the Short-Side-Chain Perfluorosulfonic Acid Membrane. *J. Phys. Chem. A* **2005**, *109*, 7583−7593.

(22) Paddison, S. J.; Elliott, J. A. On the Consequences of Side Chain Flexibility and Backbone Conformation on Hydration and Proton Dissociation in Perfluorosulfonic Acid Membranes. *Phys. Chem. Chem. Phys.* **2006**, *8*, 2193−2203.
(23) Paddison, S. J.; Elliott, J. A. The Effects of Backbone Conformation on Hydration and Proton Transfer in the "Short-Side-Chain" Perfluorosulfonic Acid Membrane. *Solid State Ionics* **2006**, *177*, 2385−2390.
(24) Wang, C.; Clark, J. K.; Kumar, M.; Paddison, S. J. An Ab Initio Study of the Primary Hydration and Proton Transfer of CF(3)SO(3)H and CF(3)O (CF(2))(2)SO(3)H: Effects of the Hybrid Functional and Inclusion of Diffuse Functions. *Solid State Ionics* **2011**, *199*, 6−13.
(25) Mayo, S. L.; Olafson, B. D.; Goddard, W. A. Dreiding: A Generic Force Field for Molecular Simulations. *J. Phys. Chem.* **1990**, *94*, 8897−8909.
(26) Daan Frenkel, B. S. *Understanding Molecular Simulation: From Algorithms to Applications*, 2nd ed.; Academic Press: San Deigo, CA, 2001.
(27) Mulliken, R. S. Electronic Population Analysis on Lcao[Single Bond]Mo Molecular Wave Functions. I. *J. Chem. Phys.* **1955**, *23*, 1833−1840.
(28) Frisch, M. J.; Trucks, G. W.; Schlegel, H. B.; Scuseria, G. E.; Robb, M. A.; Cheeseman, J. R.; Scalmani, G.; Barone, V.; Mennucci, B.; Petersson, G. A.; et al. *Gaussian 09*, revision B.01; Gauussian, Inc.: Wallingford, CT, 2009.
(29) Jang, S. S.; Molinero, V.; Cagin, T.; Goddard, W. A. Nanophase-Segregation and Transport in Nafion 117 from Molecular Dynamics Simulations: Effect of Monomeric Sequence. *J. Phys. Chem. B* **2004**, *108*, 3149−3157.
(30) Hristov, I. H.; Paddison, S. J.; Paul, R. Molecular Modeling of Proton Transport in the Short-Side-Chain Perfluorosulfonic Acid Ionomer. *J. Phys. Chem. B* **2008**, *112*, 2937−2949.
(31) Jang, S. S.; Blanco, M.; Goddard, W. A.; Caldwell, G.; Ross, R. B. The Source of Helicity in Perfluorinated N-Alkanes. *Macromolecules* **2003**, *36*, 5331−5341.
(32) Wu, Y. J.; Tepper, H. L.; Voth, G. A. Flexible Simple Point-Charge Water Model with Improved Liquid-State Properties. *J. Chem. Phys.* **2006**, *124*, 024503.
(33) Levitt, M.; Hirshberg, M.; Sharon, R.; Laidig, K. E.; Daggett, V. Calibration and Testing of a Water Model for Simulation of the Molecular Dynamics of Proteins and Nucleic Acids in Solution. *J. Phys. Chem. B* **1997**, *101*, 5051−5061.
(34) Karo, J.; Aabloo, A.; Thomas, J. O.; Brandell, D. Molecular Dynamics Modeling of Proton Transport in Nafion and Hyflon Nanostructures. *J. Phys. Chem. B* **2010**, *114*, 6056−6064.
(35) For the MSD calculations of reactive SPC/Fw water, if a water molecule accepts a proton to become a "pivot (most probable)" hydronium, the proton donor, which has been the original pivot hydronium, takes over the water's idenitity and the trajectory is continued at the donor's location.
(36) Ochi, S.; Kamishima, O.; Mizusaki, J.; Kawamura, J. Investigation of Proton Diffusion in Nafion (R) 117 Membrane by Electrical Conductivity and NMR. *Solid State Ionics* **2009**, *180*, 580−584.
(37) Zawodzinski, T. A.; Springer, T. E.; Davey, J.; Jestel, R.; Lopez, C.; Valerio, J.; Gottesfeld, S. A Comparative Study of Water-Uptake by and Transport through Ionomeric Fuel-Cell Membranes. *J. Electrochem. Soc.* **1993**, *140*, 1981−1985.
(38) Hamrock, S. J. *Final Report—Membranes and Mea's for Dry, Hot Operating Conditions*; Technical Report DOE/GO/17006-1; U.S. Dept. of Energy: Washington D.C., 2011.
(39) Pivovar, A. A.; Pivovar, B. S. Dynamic Behavior of Water within a Polymer Electrolyte Fuel Cell Membrane at Low Hydration Levels. *J. Phys. Chem. B* **2005**, *109*, 785−793.
(40) Perrin, J. C.; Lyonnard, S.; Volino, F. Quasielastic Neutron Scattering Study of Water Dynamics in Hydrated Nafion Membranes. *J. Phys. Chem. C* **2007**, *111*, 3393−3404.
(41) John, O'M. Bockris, A. K. N. R. *Modern Electrochemistry 1: Ionics*, 2nd ed.; Plenum Press: New York, 1998.
(42) Pivovar, B. S.; Smyrl, W. H.; Cussler, E. L. Electro-Osmosis in Nafion 117, Polystyrene Sulfonic Acid, and Polybenzimidazole. *J. Electrochem. Soc.* **2005**, *152*, A53−A60.
(43) Zawodzinski, T. A.; Neeman, M.; Sillerud, L. O.; Gottesfeld, S. Determination of Water Diffusion Coefficients in Perfluorosulfonate Ionomeric Membranes. *J. Phys. Chem.* **1991**, *95*, 6040−6044.
(44) Kim, M.-H.; Glinka, C. J.; Grot, S. A.; Grot, W. G. Sans Study of the Effects of Water Vapor Sorption on the Nanoscale Structure of Perfluorinated Sulfonic Acid (Nafion) Membranes. *Macromolecules* **2006**, *39*, 4775−4787.
(45) Devanathan, R. Recent Developments in Proton Exchange Membranes for Fuel Cells. *Energy Environ. Sci.* **2008**, *1*, 101−119.
(46) Feng, S.; Voth, G. A. Proton Solvation and Transport in Hydrated Nafion. *J. Phys. Chem. B* **2011**, *115*, 5903−5912.
(47) Kreuer, K. D. On the Development of Proton Conducting Polymer Membranes for Hydrogen and Methanol Fuel Cells. *J. Membr. Sci.* **2001**, *185*, 29−39.
(48) Petersen, M. K.; Voth, G. A. Characterization of the Solvation and Transport of the Hydrated Proton in the Perfluorosulfonic Acid Membrane Nafion. *J. Phys. Chem. B* **2006**, *110*, 18594−18600.
(49) Giffin, G. A.; Haugen, G. M.; Hamrock, S. J.; Di Noto, V. Interplay between Structure and Relaxations in Perfluorosulfonic Acid Proton Conducting Membranes. *J. Am. Chem. Soc.* **2012**, *135*, 822−834.
(50) Feng, S.; Savage, J.; Voth, G. A. Effects of Polymer Morphology on Proton Solvation and Transport in Proton-Exchange Membranes. *J. Phys. Chem. C* **2012**, *116*, 19104−19116.